5.5 THE ORGANIZATION AND STRUCTURE OF MESOSCALE CONVECTION DURING THE SOUTH CHINA SEA MONSOON EXPERIMENT (SCSMEX)

Jian-Jian Wang
Goddard Center for Earth Science and Technology, University of Maryland Baltimore County
Mesoscale Atmospheric Processes Branch, NASA/Goddard Space Flight Center, Greenbelt, Maryland

1. INTRODUCTION

Influenced by the largest continent—Eurasia and the largest ocean—Pacific on the earth, the East Asia monsoon becomes the most complex monsoon system. In summer, the East Asia monsoon circulation is characterized by the southwesterly flow at the low level (850hPa) and northeasterly flow at upper level (200hPa). The heavy rainfalls associated with the summer monsoon, e.g. Mei-Yu in the Yangtze Valley of China and Baiu in Japan, are important to many Southeast and East Asian countries.

Given the importance of the East Asia summer monsoon, great attention has been given to their description and investigation. Numerous studies have focused on the many aspects and components of the East Asia summer monsoon including the climatology of wind fields (e.g. Fu et al. 1983, Krishnamurti 1985, Tao and Chen 1987), the advance and retreat of the monsoon systems (e.g. Tu and Huang 1944, Ding 1994), the seasonal and annual variation of monsoon rainfall (e.g. Ninomiya and Murakami 1987, Lau et al. 1988), and the effects of Tibet Plateau (e.g. Murakami and Ding 1982, He et al. 1987). Nevertheless, many important issues related to the East Asia summer monsoon, such as the physical mechanisms involved in the onset and maintenance of summer monsoon, the influences of the mid-latitude disturbance, and the progression of the heavy rainfall are not clear. Although the heavy rainfall in Mei-Yu or Baiu season usually occur in June, the summer monsoon rainfall in East Asia starts about a month earlier in Indochina and South China Sea (SCS) area. This summer monsoon region including the SCS and surrounding landmasses is referred to as the South East Asian Monsoon (SEAM). Better understanding of the characteristics of the rainfall organization and structure in the early monsoon season will extend our knowledge on the formation and maintenance of the heavy rainfall event during the monsoon season. The organization and evolution of convection is of considerable interest because it lies at the heart of heat, moisture and momentum fluxes. It is believed to be a zeroth-order problem that must be understood before appropriate parameterizations can be developed for use with global models. However, comparing to the numerous studies focusing on the planetary and synoptic scale phenomena associated with monsoon activity, little attention have been given to mesoscale aspects of precipitating systems, especially the monsoon convection during the early stages.

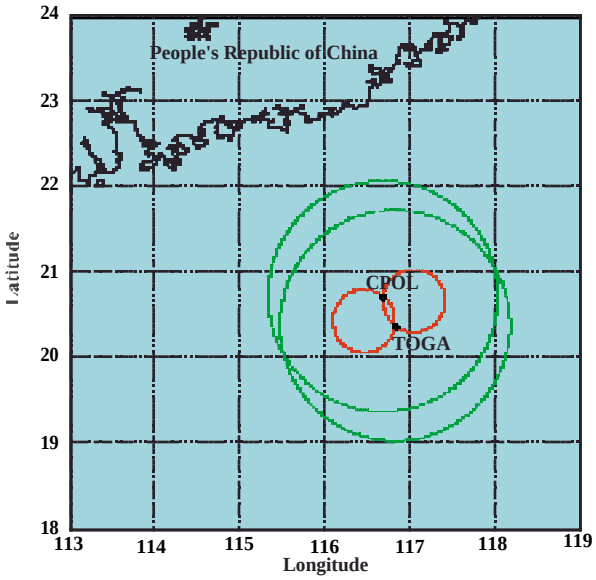

Fig. 1 Dual-Doppler radar network during SCSMEX. The green circles indicate the radar observing domain, while the red circles show the dual-Doppler radar analysis regime.

The Asia summer monsoon starts from the onset of SEAM (Tao and Chen 1987). However, the SCS area was the last area in the Asian monsoon region without a systematic observation and research. As traditional observational network is far from being adequate, the lack of observation becomes a main hamper to the research on SEAM and related physical processes. The South China Sea Monsoon Experiment (SCSMEX) was an international field experiment conducted in SCS and surrounding areas during May—June 1998. The primary goal of the experiment was to provide a better understanding of the key physical processes for the onset, maintenance and variability of the monsoon over the Southeast Asia and southern China leading to improved monsoon predictions (Lau et al. 2000). Meanwhile, as the first comprehensive field experiment aiming on the SEAM, the goal of the mesoscale program was to define the initiation, structure, evolution and dynamics of precipitation processes associated with the onset and mature phase of the SEAM. The main method to accomplish this objective was the deployment of two Doppler radars to form a dual-Doppler radar analysis region (Fig. 1) in the northern SCS. Other conventional meteorological observations including rawinsonde, surface observation network, and rain gauges were also collected on the

radar sites and surrounding areas. This observation platform allows us for the collection of a comprehensive dataset to describe the precipitation and kinematic structure, their evolution and environment of the monsoon convective systems.

Through a review of precipitating systems during the first Intensive Observation Period (IOP, 5-25 May 1998), we found that there were two types of MCS over the SCS during monsoon onset. The first type was the well-organized cloud system related to the frontal systems from northwestern China, e.g., the case of 15 May. The MCS had a large areal coverage with wide spread rainfall. On its way to the SCS, the convection might have reorganized with different orientation and propagation. An enhancement of the intensity and the formation of new convection might have also occurred. The second type was related to the mesoscale vortex that developed in northern Indochina peninsula and southern China. Periodically, when the mesoscale vortex drifted eastward along with the southern branch of westerlies around Tibet Plateau, it sometimes resulted in the eruption of convection in the northern SCS to the east of the vortex. The associated precipitation process usually consisted of several convective complexes, having either a linear or non-linear structure. The associated rainfall was relatively localized but with great intensity, e.g., the case of 24 May. In this study, case studies of 15 and 24 May on the organization and structure of mesoscale convection will be reported.

2. DATA ANALYSIS

The primary data used in this study are SCSMEX radar data, synoptic reanalysis charts from National Center for Environmental Prediction (NCEP), Geosynchronous Meteorological Satellite (GMS-5) imagery, sounding network, and automatic weather stations (AWS). During SCSMEX, the National Oceanographic and Atmospheric Administration (NOAA)/Tropical Oceans Global Atmosphere (TOGA) radar and Bureau of Meteorology Research Centre (BMRC, Australia) polarimetric C-POL radar were deployed to form a dual-Doppler radar network. The C-POL radar was installed at Dongsha Island (20.7°N, 116.7°E) and operated on a 24-h basis (with several short breaks) throughout May and June 1998. The TOGA radar was installed on the People's Republic of China *Shiyan* #3 research vessel (about 20.4°N, 116.8°E) and operated continuously during the two IOPs (5-25 May and 5-25 June). The length of radar baseline was about 40-45 km, a frequently used range to provide a good areal coverage with reasonable spatial resolution. The typical scanning procedure during SCSMEX involved a 10-min 360° surveillance scans at 15 elevations from 0.5° to 30°. Over this period, the target mesoscale system studied was assumed stationary.

The main approach of the radar data analyses in this study is the traditional "dual-Doppler" synthesis methods. After the experiment, it was determined that TOGA reflectivities were reduced about 13-16 dBZ because of a misaligned bandpass filter. In this study only the reflectivity data from C-POL were used. Three-dimensional kinematic fields were obtained by synthesizing the radial velocity measurements from the two radars within the analysis domain using NCAR Custom Editing and Display of Reduced Information in Cartesian space program (CEDRIC, Mohr et al. 1986). In our dual-Doppler radar analysis, the horizontal grid spacing was 1.5 km, and the vertical grid spacing was 0.75 km. The radial velocity analysis was advected to a common time, generally close to the middle of each volume. Vertical motion was calculated from the divergence field at each level using the anelastic continuity equation and the upward integration method. The upward integration method was required mainly because of the poor sensitivity of TOGA radar in the upper levels with weak reflectivity. Note that a 13-16 dBZ low bias in from TOGA reflectivity not only underestimated the reflectivity, but also caused a much smaller data coverage in the areas with weak echoes because the noise threshold was performed at a much higher level than expected. The missing data at the top levels may cause an inaccurate estimation of kinematic field. As a result, the upper boundary condition was hard to define. Without the establishment of the upper-boundary conditions, the estimation of vertical velocity using upward integration in this study is subject to some uncertainty.

To filter noise in the vertical velocities, the horizontal wind fields derived from the dual-Doppler solution are lightly smoothed with a two-pass Leise filter (Leise 1981) prior to divergence calculation and vertical integration. This procedure significantly damps wavelengths up to 6.0km and removes wavelengths of less than 4.5km. The storm motion vector was calculated by inspection of the leading edge of the convection in sequential horizontal cross-section of low-level reflectivity.

3. RAINFALL DEVELOPMENT DURING THE SCSMEX AND BEYOND

In this paper, to avoid the confusion of monsoon flow and monsoon rain which may not always be positively correlated, *pre-onset* and *post-onset* are used to indicate the stages before and after the setup of monsoon (flow) circulation with *onset* (transition) period in between, while *active* and *break* are used to indicate the periods with heavy and little monsoon rain, respectively, *after* the monsoon onset. Rainfall recorded by the rain gauge at Dongsha Island throughout the SCSMEX IOPs (Fig. 2) can be clearly divided into several periods related to the different stages of monsoon onset. Prior to 15 May 1998, the SCS region was mainly under the control of the

subtropical high over the western Pacific. On the western flank of the subtropical high, low-level airflow at 850 hPa exhibited southeasterly winds in the southern SCS and southwesterly winds in the northern SCS (Fig. 3a). At the 200-hPa level, there was an anticyclone located on the Bay of Bengal (Fig. 3b). Under its influences, the northerly flow was observed on SCS. Since the beginning of the first IOP, the frontal passages from northwestern China to the coastal regions were observed periodically with an interval of 2-4 days. The well-developed frontal cloud/rain bands usually extended from south China along the coast to Korea Peninsula and Japan. An example of this type of frontal system on 11 May was shown in Fig. 4a. However, once the southern part of the frontal systems passed China coast into the northern SCS, the cloud/rain bands associated with the front weakened and dissipated without generating any organized precipitation in the area (Fig. 4b). The divergence showed a low-level divergence and upper-level convergence on 11 May (Figs. 3a and 3b) consistent with suppressed convection. In general, during the pre-onset period prior to 15 May, suppressed conditions were observed for the most of time over SCS with little rain. Convection was primarily in the form of scattered precipitating congestus, with isolated cumulonimbus cells.

The large-scale wind fields started to change, especially at low levels, in the northern SCS on 15 May. At 850 hPa, comparing to the wind fields days before, the western Pacific subtropical high retreated eastward (Johnson and Ciesielski 2002) and a cyclonic system developed in the eastern China. More important, there were two more branches of airflow joining the existing southwesterly flow. The first branch originated in the Bay of Bengal to the east of the equatorial twin cyclone (only the northern cyclone centered near 10°N and 82°E shown in Fig. 3c). The second branch was the cross equatorial airflow, originating in the Australian region in the Southern Hemisphere. These two airflows are the main components forming the East Asia summer monsoon (Tao and Chen 1987). The equatorial flows merging into the northern SCS region also resulted in an increase of relative humidity to over 70% (not shown). The rapid increase of the relative humidity was a significant mark of the onset of SEAM. At 200-hPa, the strong anticyclone continuously dominated the Indo-China region and the surrounding Bay of Bengal and SCS area to form a diffluent field (Fig. 3d). As a result, the wind fields shifted to low-level convergence and upper-level divergence (Figs. 3c and 3d) more favorable to the formation of convection. On 13 May, a frontal system migrated southeastward from mainland China. A pronounced frontal system oriented from southwest to northeast covered most coastal regions of southeastern China at 0000 UTC (LST = UTC + 8 h) 15 May (Fig. 4c). Different from the frontal system reaching coastal region four days earlier, this system was able to move into the sea without any weakening. It is interesting to note that after the start of summer monsoon onset in the northern SCS, the frontal cloud bands even enhanced its intensity and areal coverage in the southern portion (partially over the northern SCS) (Fig. 4d).

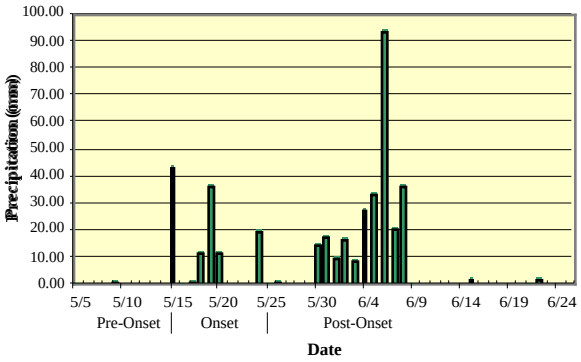

Fig. 2 Daily rainfall recorded at Dongsha Island.

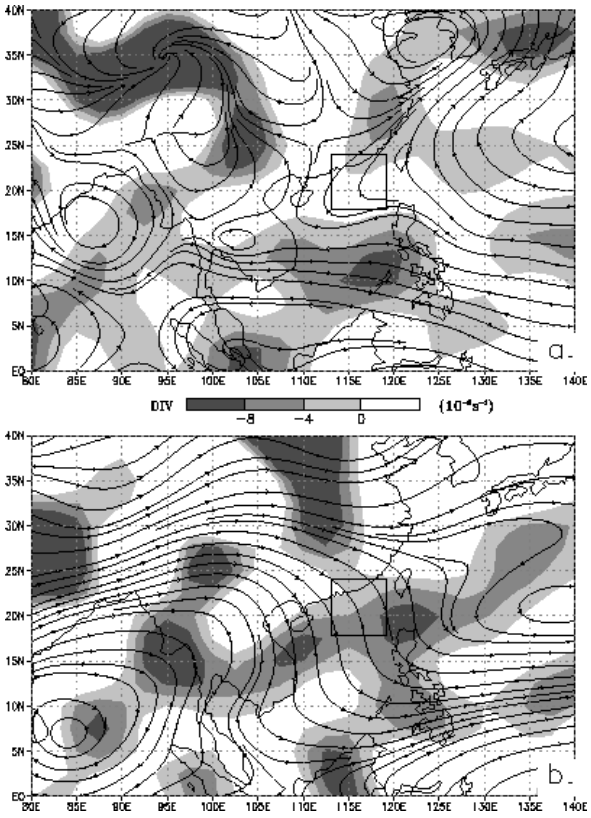

Fig. 3 NCEP constant pressure level reanalysis at (a) 850 hPa, (b) 200 hPa valid at 0000 UTC 11 May, (c) 850 hPa (heavy solid line indicate the position of front), (d) 200 hPa valid at 0000 UTC 15 May, (e) 850 hPa, (f) 200 hPa valid at 0000 UTC 20 May, (g) 850 hPa, (h) 200 hPa valid at 0000 UTC 24 May, (i) 850 hPa, (j) 200 hPa valid at 0000 UTC 5 June. The square denotes the domain shown in Fig. 1.

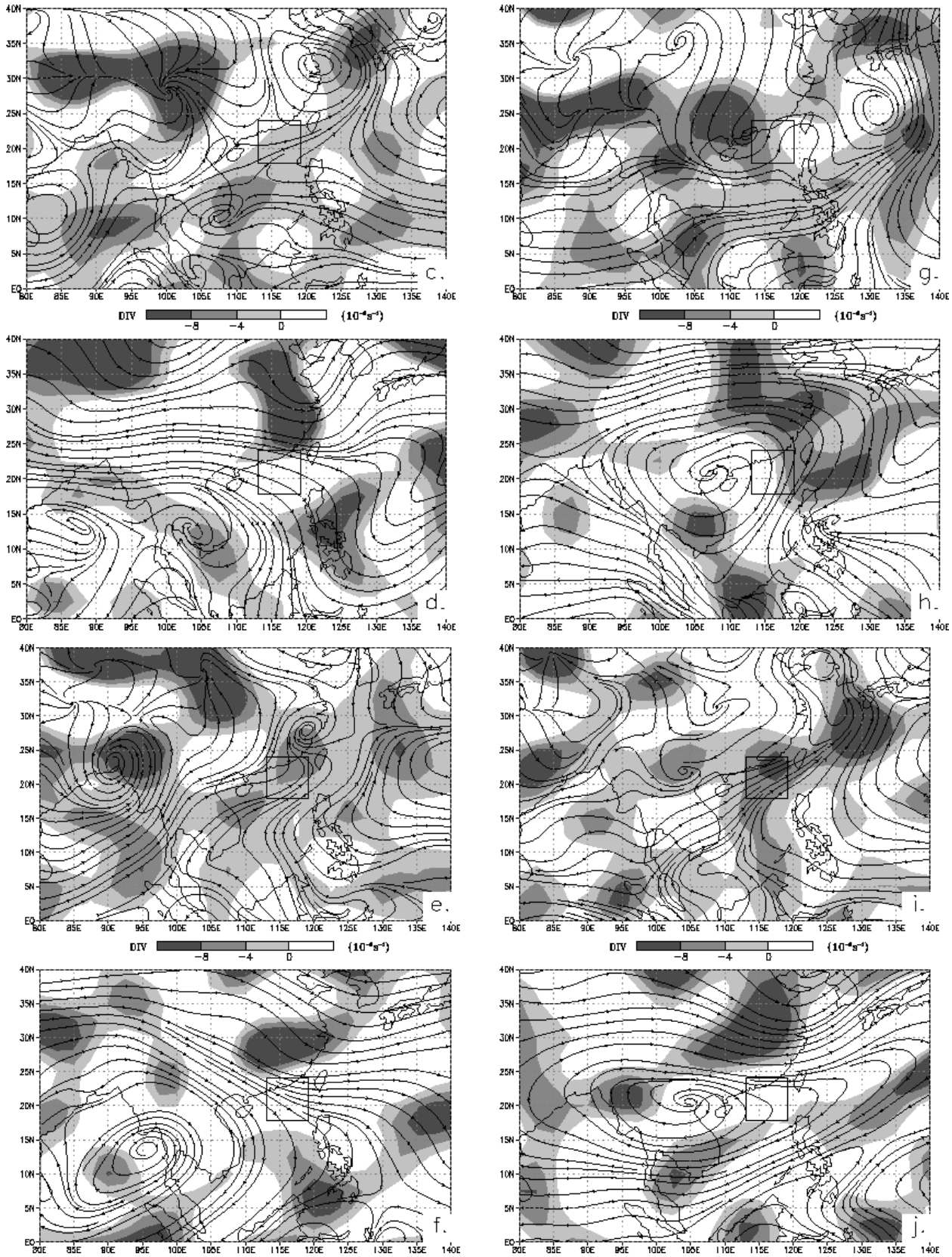

Fig. 3 *Continues.*

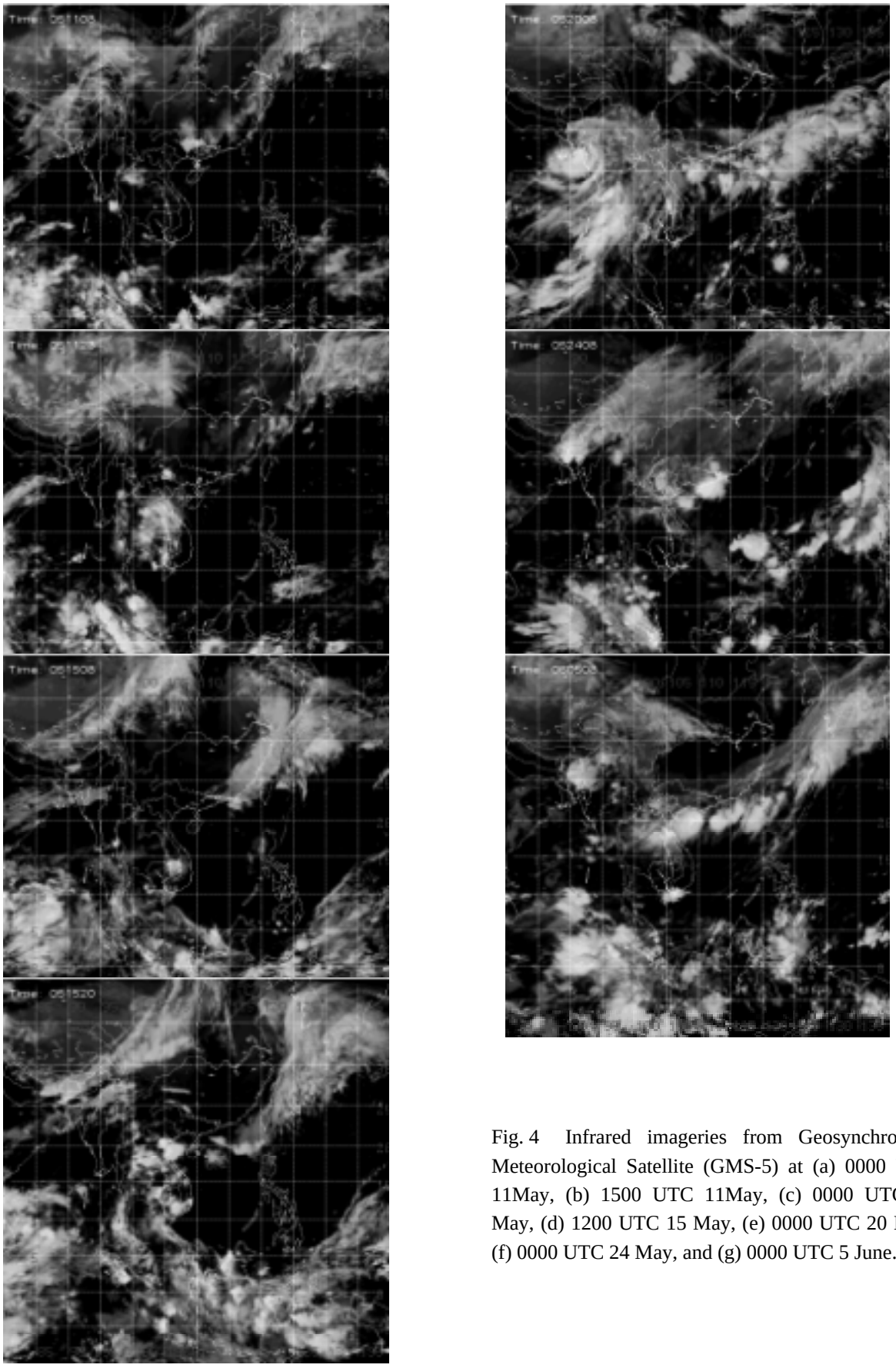

Fig. 4 Infrared imageries from Geosynchronous Meteorological Satellite (GMS-5) at (a) 0000 UTC 11May, (b) 1500 UTC 11May, (c) 0000 UTC 15 May, (d) 1200 UTC 15 May, (e) 0000 UTC 20 May, (f) 0000 UTC 24 May, and (g) 0000 UTC 5 June..

It is important to note that at its early stage, the onset of the summer monsoon (transition period) only occurred partially in the northern SCS. The low-level airflow in the southern SCS remained southeasterly (Fig. 3c). Therefore, the convection associated with the frontal passage on 15 May was limited in the northern SCS area, and failed to penetrate further south (Fig. 4d). The establishment of summer monsoon at low-level over the SCS did not occur until 20 May (Fig. 3e), while the southwesterly airflow from the equatorial regions prevailed in the whole SCS. At that time, when another frontal system coming from mid-latitude, along with the progression of monsoon onset, the frontal cloud bands experienced a significant enhancement after moving southeastward to the sea (Fig. 4e). Compared to the frontal passage on 15 May, with the completion of SEAM onset at low levels and the increase of upper-level diffluent flow (Fig. 3f), the convection accompanying the frontal system had a broader areal coverage. The precipitation system did not only produce rainfall in the northern SCS region, but also extended to southern SCS. After moving into the SCS, the cloud systems associated with the front stayed in the SCS longer, continuously generating three days of rainfall (18-20 May, Fig. 2) in the region.

After the setup of southwesterly monsoon flow at low-level, the shift of the upper level wind began in SCS. The anticyclone at 200 hPa over Indo-China experienced a northward jump after 20 May. On 24 May, the upper level anticyclone was centered near 21ºN and 107ºE (Fig. 3h). This was consistent with the results from summer MONEX (He et al. 1987) that the south Asian anticyclone at 200 hPa abruptly moved northward from 10° to 20°N in May. As a result, the northeasterly winds dominated the upper level circulation over the SCS region. This was also the indication that the transition period for the onset of SEAM, i.e., the set up of tropical southwesterly flow at lower troposphere accompanied by the northeasterly anticyclonic flow at upper troposphere (Figs. 3g and 3h), was completed. Meanwhile, a mesoscale vortex originated from northern Indochina peninsula propagated eastward to the SCS region (Fig. 4f). A tall and well-organized oceanic squall line system associated with the vortex was also observed by radar network after 1200 UTC 24 May.

Overall, the onset of SCS summer monsoon in 1998 started in the northern SCS on 15 May, progressed to central and southern SCS on 20 May, and completed near 24 May. This type of two-stage, north to south, SCS monsoon onset is neither typical nor very unusual. It happens in 13 of the 47 years (27.6%) from 1953 to 1999 (Ding and Liu 2001). In addition, the SCS summer monsoon onset in 1998 was among those years with late onset. The mean onset of SCS summer monsoon occurred during 5-15 May (Tao and Chen 1987, Ding and Liu 2001). From rainfall data collected at Dongsha Island, the post-onset period in SCS starting on 25 May following the 10-day transient period included a short break period, a 10-day active rainy period, and finally a long break period to the end of SCSMEX and beyond (Fig. 2). The short break period of 25-30 May appeared to be related to the lack of synoptic-scale disturbance. From 30 May to 10 June, significant rainfall amount was recorded almost continuously (Fig. 2). At 200 hPa (Fig. 3j), when the anticyclone over Indochina oscillated around 20°N, the southern SCS was controlled by the persistent northeasterly flow. However, the northern SCS region at the northeast corner of the anticyclonic circulation was often in a divergent westerly flow. The general mechanism, a stable low-level convergence zone between the southerly summer monsoon and northerly flow from mid-latitude (Fig. 3i), responsible for the stable rain band during the early June in the northern SCS region (Fig. 4g) was very similar to that of the Mei-Yu frontal rainfall affecting mainland China and Japan in later summer monsoon season (Chen 1993, Ding 1994). Since 10 June, along with the northward jump of the Pacific subtropical high, the semi-permanent rain belt leaped to southern China for the start of Mei-Yu season there. Meanwhile, the rainy period over SCS region ended with mostly clear sky, although the low-level southwesterly summer monsoon dominated the region.

4. RAINFALL CHARACTERISTICS AND KINEMATIC STRUCTURE

4.1 *Case of 15 May*

On 15 May at the beginning of summer monsoon onset, the first intense MCS in the SCS regime was observed during SCSMEX. It was also recorded as the rainiest day at Dongsha Island during the first IOP with 43mm precipitation (Fig. 2). At 0000 UTC 15 May, a frontal system was evident in the coastal region of eastern China from both synoptic charts and satellite imagery (Figs. 3c, 3d, 4c).

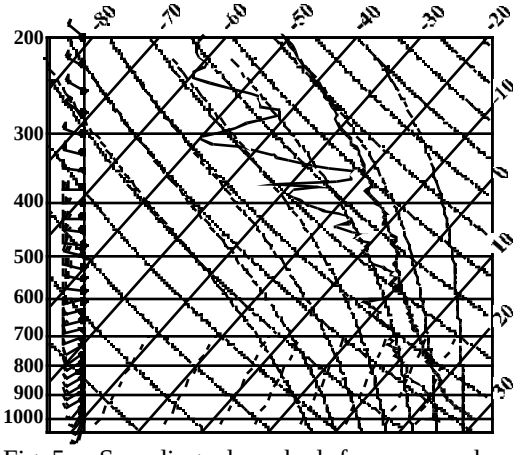

Fig. 5 Soundings launched from research vessel Shi Yan #3 at 0600UTC (solid lines) and Dongsha Island at 1200 UTC (dashed lines), 15 May 1998.

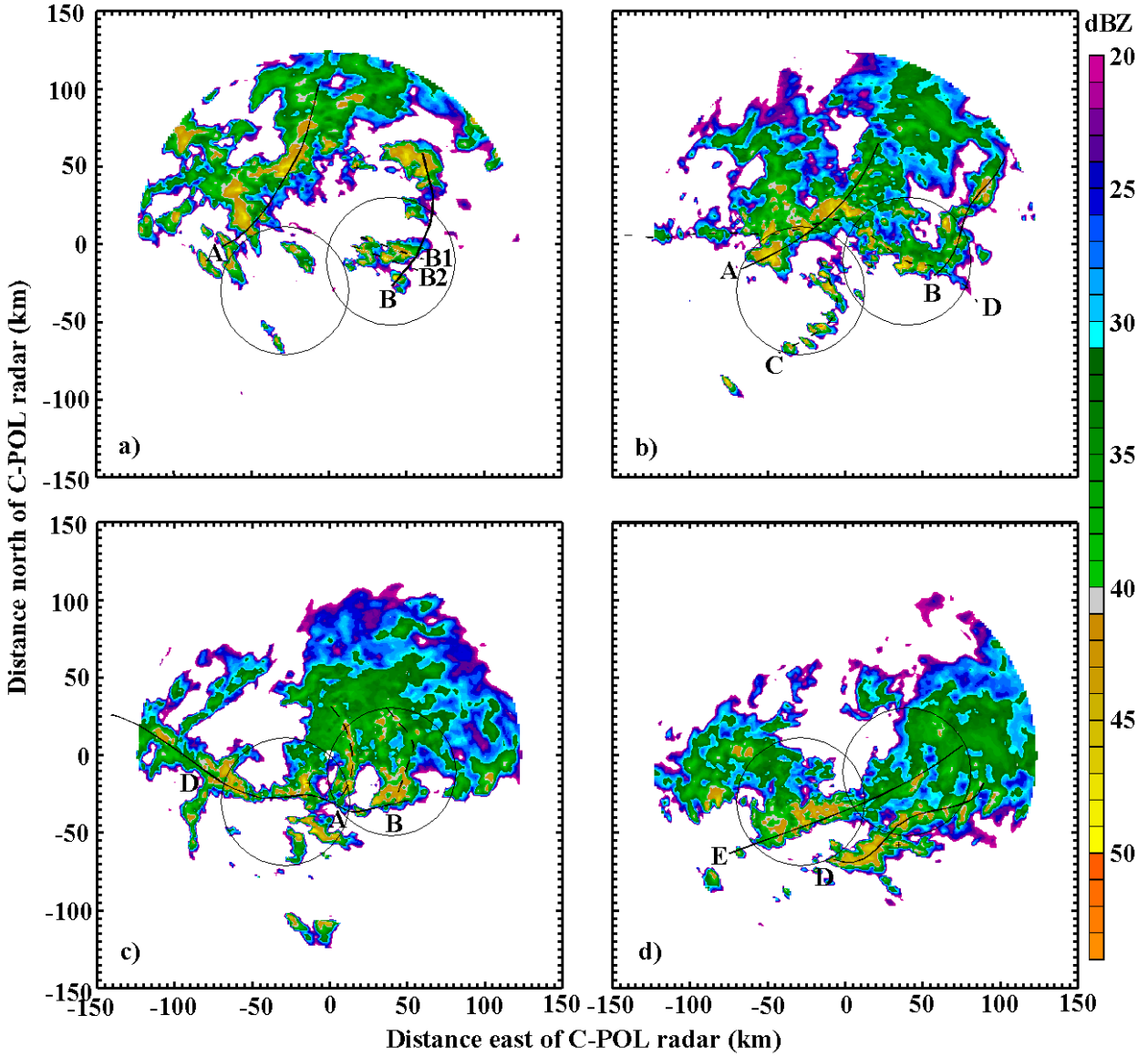

Fig. 6 CPOL radar reflectivity (dBZ) at 2.5 km MSL at (a) 0600 UTC, (b) 0700 UTC, (c) 0830 UTC, and (d) 0930 UTC, 15 May 1998. The reflectivity is shaded as shown to the right. The main convective lines are denoted by solid line, while the secondary convective lines are indicated by dash line.

At 0600 UTC, the main feature in the radar domain was the linear northeast to southwest oriented frontal rainband with a width of about 40 km (A in Fig. 6a). The present rainband had a maximum radar reflectivity over 50 dBZ and was close to the front at 850-hPa. Ahead of the convective line A, there were two groups of newly formed convection at 50 km east to C-POL. Johnson and Keenan (2001) noted that the convection in the pre-frontal region might orient relative to the low-level and/or mid-level wind shear. The primary convective line ahead of the frontal rainband (B in Fig. 6a) was oriented north south (Fig. 7a), while the secondary convective line (B1 and B2 in Fig. 6a) located in the middle of east dual-Doppler lobe was oriented east west. In their studies on western Pacific convection, LeMone et al. (1998) found the orientation of the convection tends to be perpendicular to the low-level wind shear if its magnitude is over 4 m s^{-1}. They also noted that the secondary lines were parallel to the low-level shear. On 15 May, the low-level vertical wind shear in the pre-frontal region is westerly with the magnitude of 5.4 m s^{-1} (Fig. 5). The orientation of convective lines was consistent with the conclusion made by LeMone et al. The convection had a larger areal coverage in an hour later at 0700 UTC (Fig. 6b). However, the northeastern portion of the convection started to weaken with more stratiform characteristics from the earlier convective lines. At the same time, between the two northeast to southwest oriented convective lines and beyond, there was a tendency to

form a narrow convective line (D in Fig. 6b) perpendicular to the earlier convective lines. This new line intensified and became the primary feature in the following hours. Another feature at 0700 UTC was the new developing convective line (C in Fig. 6b) in the pre-frontal region with low-level southwesterly winds prevailing (not shown). The development and structure of this convective line were very similar to the early formed pre-frontal MCS (B in Fig. 6) which will be analyzed in detail in section 4b.

The front at 850-hPa passed the C-POL at about 0730 UTC. In the next hour, the orientation of the main convective line exhibited a dramatic change. As shown in Fig. 6c, the main radar echo became an east-west oriented convective line across the dual-Doppler radar analysis region. This was the convective line started to form at 0700 UTC (Fig. 6b) in the post-frontal region. The dominated northeast to southwest oriented convective lines in earlier hours weakened during the same period. The area with radar reflectivity over 40 dBZ reduced remarkably. Two weak north-south oriented lines existed to the north of main convection as the residual from the early convection. A large area of stratiform precipitation of the pre-frontal convection was also observed in the northeast quadrant. During SCSMEX, this type of sharp change of convection orientation in a time spread of several hours was also frequently observed in other cases. At 0930 UTC, the north south oriented convective lines continued to dissipate with some stratiform precipitation remaining. On the contrary, the primary east-west oriented convective lines became more pronounced showing increased areal coverage and enhanced intensity (Fig. 6d).

A vertical cross-section through the convective line to the east and two convective cells to the west is made to characterize the structure of airflow and vertical circulation. We will focus on the cell in the convective line, about 50 km east to C-POL, which was well developed with largest east-west extension. Compared to the typical rearward sloping structure observed in the tropical linear convection (e.g. Jorgenson et al. 1997), a notable characteristic of this convective line was that the reflectivity pattern was almost straight upward without much slope. This type of precipitation with little tilt was often found in an environment without strong vertical wind shear (Fig. 5). During the summer monsoon onset period in 1998, the westerly winds

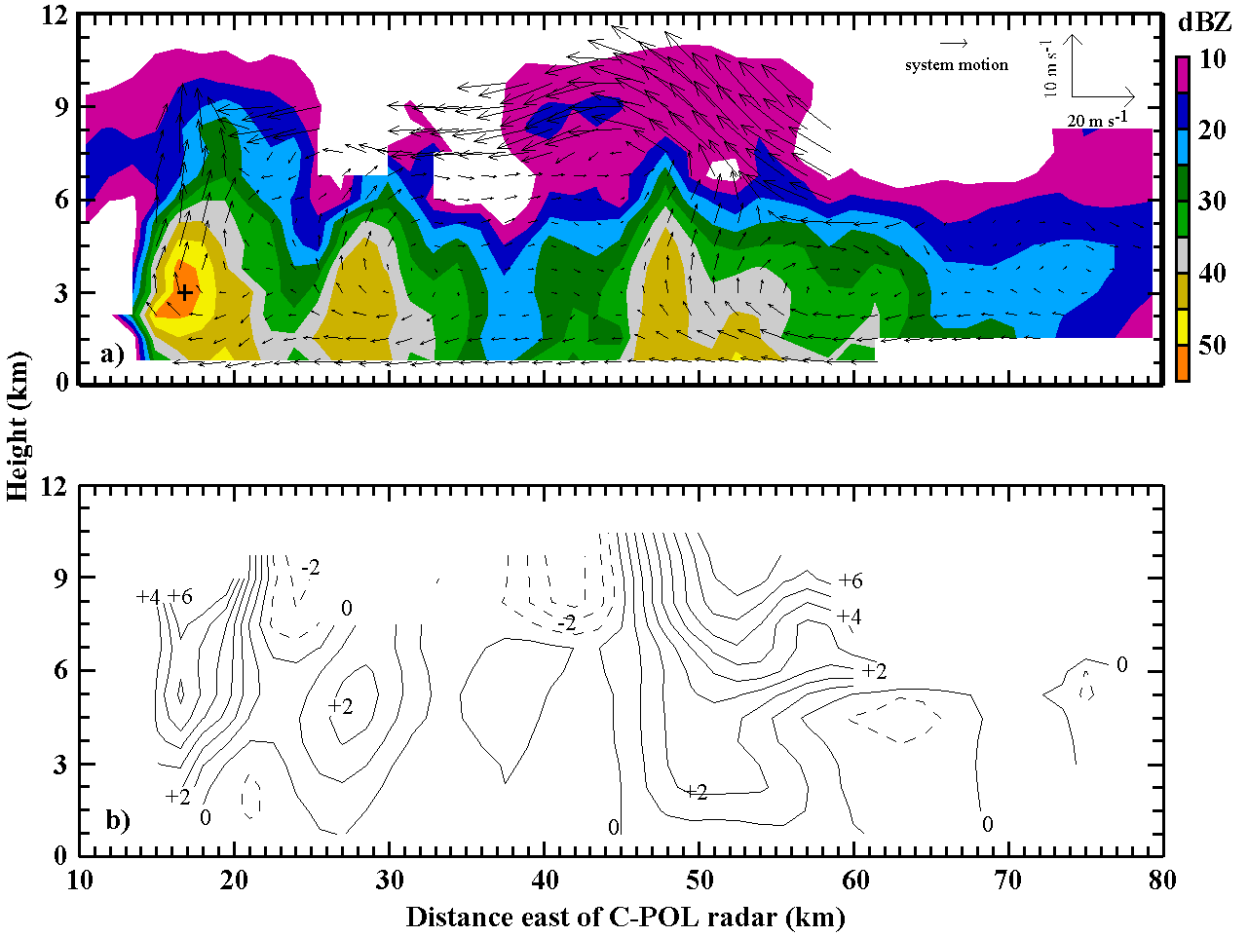

Fig. 7 Vertical cross section of (a) reflectivity and line-normal system relative wind and (b) vertical motion (m s-1) at Y=-8.5km valid at 0620 UTC.

generally dominated through the whole convective layer as the onset of upper-level northeasterly occurred at the end of transition. As a result of limited vertical wind shear, the straight upward echo pattern with little tilt was commonly observed during the period. The echo top, denoted by 10 dBZ reflectivity isopleth, was at about 11 km MSL. The front to rear low-level inflow started from the lowest level with the maximum strength below 1.5 km MSL. However, maximum low-level convergence and updraft did not occur in a narrow ribbon within 1-2 km to the leading edge as other tropical convective lines (LeMone et al. 1984, Jorgenson et al. 1997). Instead, they were in the rear part of the convection (45-50km east to CPOL) about 20-30 km behind the leading edge (70-75 km east to CPOL). Numerous studies emphasized the important role played by the cold pool and the convective downdraft in the maintenance of the convection (Waikimoto 1982). The evaporative cooling of raindrops results in cool air brought down to surface in the form of convective downdrafts. Downdrafts spread at the ground and carry some of the momentum from middle levels, thereby enhancing the convergence at the outflow boundary. For those tropical MCSs with maximum updraft at the leading edge, the systematic downdraft was located immediately following the leading edge. However, the cross-sections of low-level divergence (not shown) and vertical velocity at 0620 UTC (Fig. 7) showed that the center of low-level divergence and downdraft was farther behind, about 7-10 km from the reflectivity maxima. This spatial distribution of the downdrafts could be a result from that the convective cell was straight upward with little tilt. In a more vertical cell, the potential downdraft near the leading edge would encounter the low-level inflow and updraft. While the downdraft was usually weaker than updraft in the convective core (LeMone and Zipser 1980), the downdraft was only found in the rear part away from the leading edge where the updraft was weak. In addition, this structure also implies that inflow must pass a raining area ahead of convective core before entering the convective towers. From a simple 2-D numerical simulation, Parker and Johnson (2001) noted that despite the low-level inflow parcels being chilled in the pre-line precipitation region, strong lifting along the edge of the cold surface outflow (i.e., the front) might be enough to bring the air parcel to the level of free convection. Thus, the cooling of inflow parcels ahead of the convective core did not appear to be a detriment to long-lived systems.

Ahead of the convective cells, system-relative westerly rear to front flow was observed at the mid-levels, blowing the particles ahead of the line (Fig. 7a). In most previous studies, the stratiform rains in the tropical convection were found behind their convective counterpart (trailing mode) as a result of the mid- to upper-level outflow in the same direction as low-level inflow (Jorgenson et al. 1997, Protat and Lemaitre 2001). However, in the pre-frontal case studied here, the stratiform rain had a tendency forming ahead of the convective rain (leading mode, Figs. 7a) in response to the mid-level "return" flow. During the onset of SCS monsoon, there was other convective cases (e.g. 24 May) showing the similar structure with leading stratiform rain. At the upper-levels, strong easterly system-relative winds dominated over the convective core (Fig. 7a). Comparing to the pre-frontal sounding (Fig. 5), these high-level easterly winds were purely convection driven as described in a two-dimensional theoretical model by Moncrieff (1992). Interestingly, with such strong system-relative easterly winds, the radar echoes at the upper levels were limited in a small area. The hydrometers were concentrated over the top of the intense convective core, but lack of an extension to the downwind side. The environmental conditions before the arrival of the frontal system showed a very dry layer at 300 hPa (~9 km MSL, Fig. 5). The dry air in the upper levels might result in a quick evaporation and sublimation of the forming stratiform cloud when the hydrometers were quickly blown from the top of the convection. The moistening at the upper levels due to the evaporation and sublimation of the hydrometers was also evident from the post-frontal sounding collected at 1200 UTC at Dongsha island (Fig. 5) which exhibited a much moister upper layer comparing to six hours earlier. Vertical motion cross section (Fig. 7b) reveals that the maximum updraft occurred just east to the reflectivity maxima, indicating a eastward propagation. When the vertical motion was integrated from horizontal winds which was a process with error accumulation, the magnitude of the vertical motion at upper-level may contain notable uncertainty due to the missing data at high-level by TOGA radar. From our synthesis, the maximum updraft was at a speed of 6.7 m s^{-1}. This moderate updraft was comparable to most tropical convection (Zipser and LeMone 1980, Jorgenson and LeMone 1989).

Fig. 8a is a vertical cross-section of radar reflectivity and system-relative motion across one of the most intense cells. The maximum reflectivity was over 55 dBZ with an echo top surpassing 12 km MSL. Comparing to the pre-frontal convection (Fig. 7), the post-frontal convection was taller and more intense. The similar contrast between the pre- and post-frontal was also found in other MCS cases related to the frontal passage, e.g., cases of 17 and 19 May, during the period of summer monsoon onset. This contrast was a result from that the low-level convergence in the post-frontal region was much stronger than that in the pre-frontal area. The cross-section of the post-frontal convection (Fig. 8) contains some of the common characteristics of tropical convection. The low-level inflow was from the warm and moist tropical air ahead of the leading edge. With the maximum low-level convergence near the narrow leading edge of the convective line, the center of the updraft was in front of the convective core.

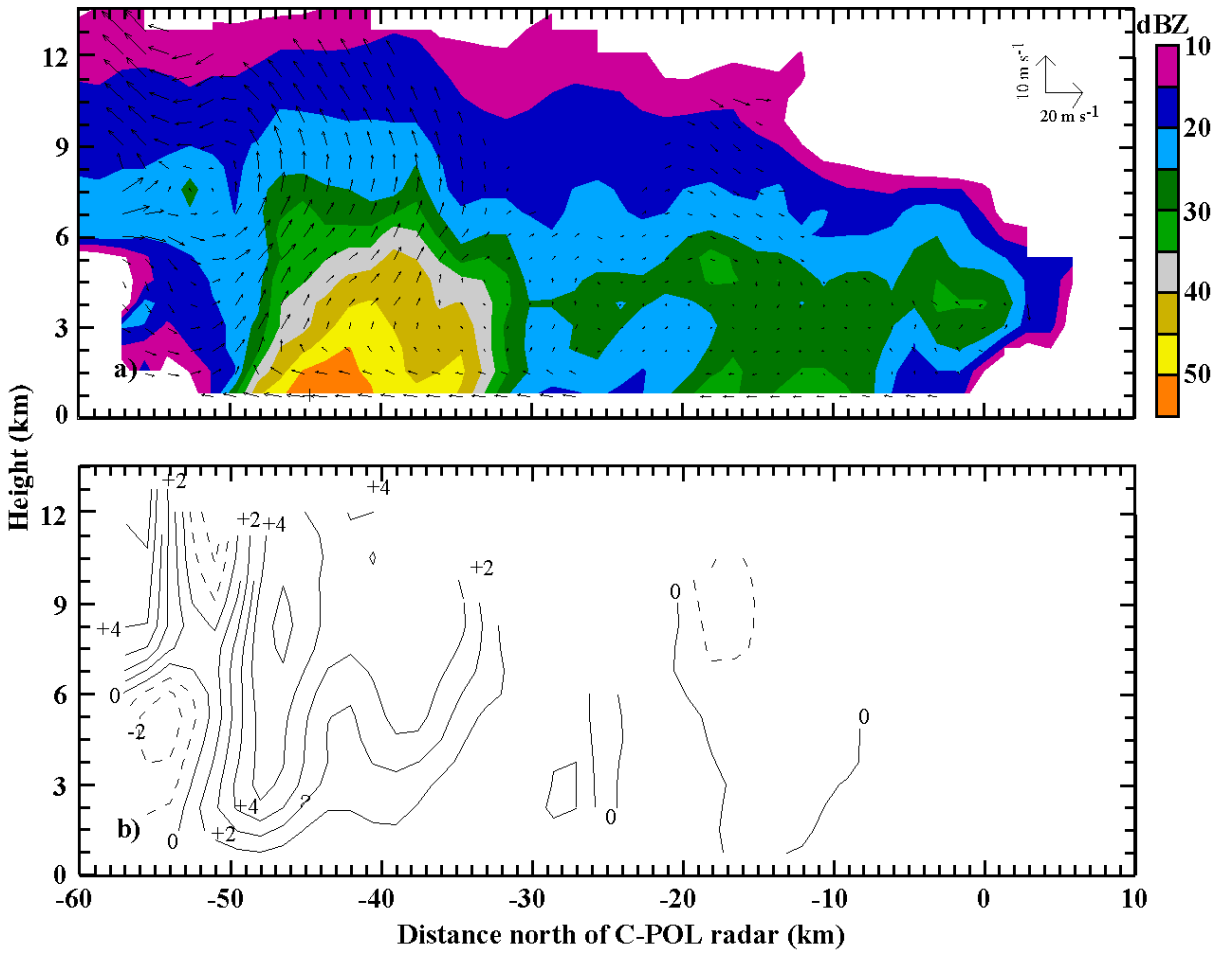

Fig. 8 Same as Fig. 7, except X=-34km valid at 0930 UTC.

There was a rapid reflectivity reduction with height above the melting level (~4.5 km MSL) as a result of relative weak updraft velocities in tropics (Zipser and LeMone 1980). The maximum updraft velocity was recorded over the convective core at an elevated height (7.5 km MSL) with a magnitude of 5.5 m s^{-1} (Fig. 8b). However, departures from the typical tropical convective line were also evident. Again, both reflectivity and vertical airflow were relatively straight upward. The upward inflow did not go through to the rear part at the upper level. Instead, it turned to a rear to front flow above 7.5 km MSL. As a result, a stratiform echo formed at upper level ahead of the convective line resulting from the frontward advection of hydrometers contributed by the relative flow across the leading edge. It should be emphasized that although both the pre-frontal and post-frontal convection exhibited a formation of leading stratiform region ahead of the convective line, there was different kinematic structure from them. In the pre-frontal convection, the stratiform rain up front was caused by the mid-level rear to front flow. Although strong front to rear flow dominated at the upper-level in pre-frontal convection, the dry environmental air near 300 hPa (Fig. 5) prevented the stratiform rain from forming in the trailing area. In the post-frontal convection, the leading stratiform rain was caused by strong rear to front upper-level outflow.

Following the 20-30 km wide convective area was an area of minimum reflectivity with descending airflow in the region. Further behind was a patch of stratiform rain. A bright band structure (~4.5 km MSL, Fig. 8a) in the reflectivity data was located at and below the melting layer. Nevertheless, the stratiform echo on the right of the cross-section was not the trailing part from the convective portion to the south. Actually, the stratiform rain was the remaining portion from the earlier convective rain. In most stratiform region, mesoscale updraft exists above the bright band while mesoscale downdraft presents below the bright band (e.g. Biggerstaff and Houze 1991). However, at the time studied here, the descending flow existed throughout the whole layer of the stratiform region. This could be a result from a decaying process of the stratiform rain, a residual from the early convection. A much lower echo top in the stratiform region than that in the convective region (Fig. 8a) was another evidence for the existence of descending flow at upper level.

4.2 *Case of 24 May*

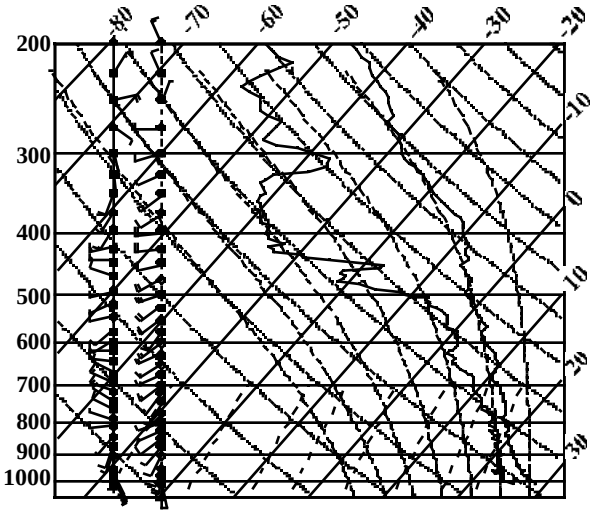

Fig. 9 Sounding launched from research vessel Shi Yan #3 at 1200UTC 24 May 1998.

The squall line system including several lines persisted from 1200 UTC 24 May to 0500 UTC 25 May. Wind and thermodynamic sounding, representative of the pre-storm environment at 1200 UTC, 3-4 h prior to the passage of the squall lines are summarized in Fig. 9. At that time, moisture was available at low-levels. A very dry layer was found at the mid- to upper-levels over 500 hPa, with a maximum dewpoint depression over 25°C around 400 hPa. The sounding exhibited conditional instability. The mesoscale structure and evolution of the squall line system during the period 1200 – 2200 UTC 24 May is shown in Fig. 10 using constant altitude plan position indicator (CAPPI) radar reflectivity fields at 2.5 km MSL. The early convective echoes appeared at about 1200 UTC as several individual newly formed convective cells. The cells to the south were relatively intense with maximum radar reflectivity reaching 40 dBZ. These small cells lined up in a discontinuous arc-shaped convective line about 50 km west of the CPOL radar (Fig. 10a). The north-south orientation of the convective line is perpendicular to the low-level wind shear (1000 to 800 hPa). This was in consistent with the studies on western Pacific convection by LeMone et al. (1998).

While moving westward, this convective line gradually intensified into a broader, stronger, and more organized squall line. At 1300 UTC, southward extension of the northern echoes was evident. An hour later, both the northern and southern portion of the squall line showed apparent enhancement and extension to the center. At 1400 UTC, a few strong echoes existed from north to south with a considerable area of radar reflectivity over 40 dBZ. This squall line reached its climax both in size and intensity near 1600 UTC. The peak reflectivity of 55 dBZ was recorded at 3km MSL with the echo top at 12km MSL. The squall line started to dissipate after 1600 UTC. From 1200 UTC to 1700 UTC, the squall line propagated northeastward at various speeds with the fastest speed of 8 m s^{-1} at the northern end and the slowest speed of 2 m s^{-1} at the southern end. Near the Dongsha Island (CPOL radar), the propagation speed was 6-7 m s^{-1} on averaged.

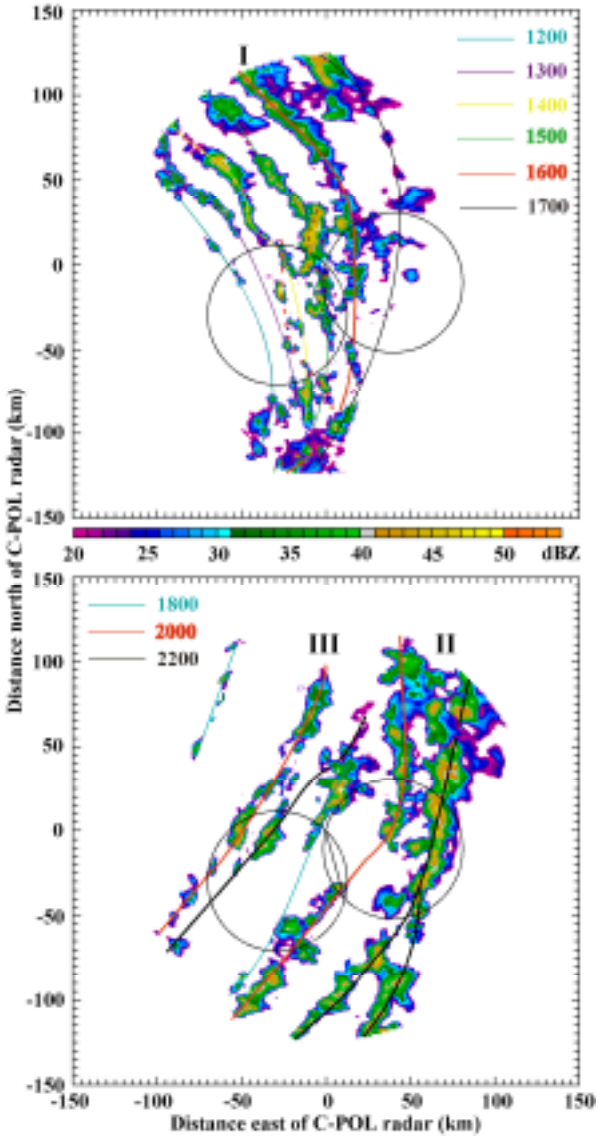

Fig. 10 Time series of the CPOL radar reflectivity (dBZ) at 2.0 km MSL for the evolution of the main echoes of (a) the first squall line, and (b) the second and third squall lines on 24 May.

Along with the decaying of the first squall line, a new and intense convective line started to develop about 40 km behind the original squall line (Fig. 10b). Compared to the echoes in the first squall line, the main echo of the second squall line at its early stage was more intense with larger area coverage. The southern portion of the second squall line began to form at 1800 UTC. From 1800 UTC to 2000 UTC, the second squall

line enhanced significantly on their way moving southeastward. At 2200 UTC, the second squall line was at its mature stage showing a continuous convective band with the east-west extension up to 50 km. The second squall line reached its climax at about 2200 UTC 24 May to 0000 UTC 25 May. The peak radar reflectivity of over 50 dBZ was recorded at 1.5-3.0 km MSL. Overall, the second squall line was much more enhanced than the first squall line in both the size and intensity. With the echo top reaching 15 km MSL, the second squall line was also the tallest convection observed on 24 May. There were two factors that may have caused the second squall line to be a much more intense line than the first one. First, the second line developed right after the midnight and throughout the early morning hours, when the diurnal cycle of the convection over the open ocean reached its most active period (Houze 1993). Second, the post-line environmental conditions with a much higher value of CAPE (not shown) was more favorable for the development of deep and intense convection. The mature phase of the second squall line lasted for several more hours till 0400 UTC 25 May and started to dissipate afterward.

About an hour later after the formation of the second squall line, to the northwest, several new cells developed to line up in the northeast to southwest direction about 80 km behind the second squall line at 1800 UTC. These cells formed a more continuous convective line later and became the third squall line observed on 24 May. In the next two hours or so, the third squall line experienced significant intensification on both the size and strength. However, after 2200 UTC when the second squall line at its mature phase, the third squall line to the west weakened to a short line and dissipated in the next hour or so. Contrasting to the well-developed second squall line, the third squall line did not reach fully development before its dissipation. Without enough data around the third line or between the second and third line, we are not sure about the cause for the dissipation of the third line. However, considering the third line was just a few tens kilometers behind the mature and intense second line, we believe that the effects of the second line may play a role in this process. For instance, the mesoscale descending motion often detected after the passage of strong convection may suppress the maintenance of updrafts and result in the weakening of the third line.

The vertical cross sections of radar reflectivity, system-relative wind, and vertical velocity across the two principal cells are shown in Fig. 11. The echo top reached 14-16 km MSL. Although not shown in our interpolation, the actual maximum radar reflectivity recorded was about 55 dBZ. An important characteristic of this squall line, similar to case of 15 May, was that the front to rear low-level inflow going all the way to very rear part of the cell. The deceleration of the low-level inflow from the front portion was also evident. The formation of a new cell behind the old cell was apparent (Fig. 11a). The low-level maximum updraft was also located at the rear of the system (Fig. 11b). This type of strong updraft at rear also implied that inflow must pass a region ahead of convective line before entering the convective tower. When the inflow passing the convective precipitating area, it could be chilled by the cool air caused by the evaporation cooling. As a result, the buoyancy of the air in the updraft might be reduced. Consequently, the intensity of the updraft and the convection might weaken as well. Different from case of 15 May, the squall line observed on 24 May was not associated with any synoptic scale forcing which may provide lifting for the low-level infow to overcome the precipitation cooling. Examining the sounding taken at Dongsha Island at 1200 UTC 24 May (Fig. 9), it was found the thermodynamic stratification was near neutral. Therefore, once the circulation started, little extra lifting would be needed to maintain it.

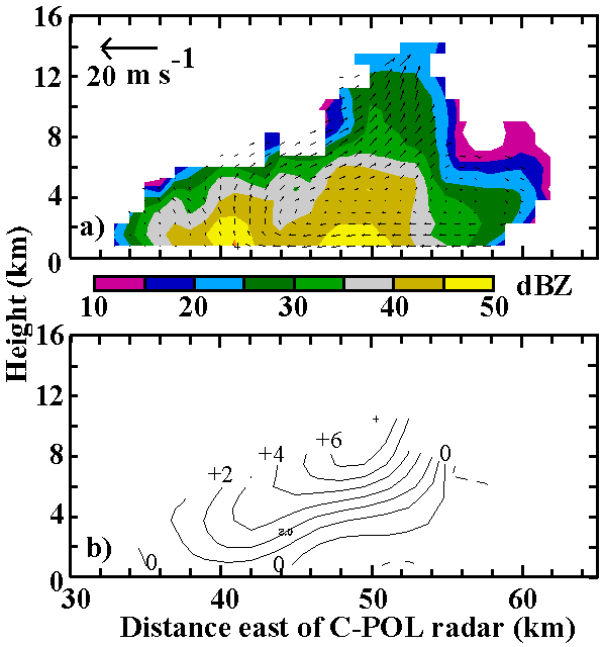

Fig. 11 Vertical cross section of (a) Radar reflectivity (dBZ) and system-relative wind flow, and (b) vertical air motion (m s-1) at Y=-17km valid at 2040 UTC.

It is also noted that due to the very dry air at the upper-levels (Fig. 4) the strong squall line had little stratiform precipitation accompanying the convective portion. In addition, the weak upper-level winds may also play a role in minimizing the scale of stratiform rain without blowing hydrometers away from the convective cores. A forward tilt of roughly 40° from the horizontal was seen in both the vertical airflow and reflectivity contours in the cross section. The maximum updraft was about 5-7 m s^{-1} at an elevated height of 9-10 km MSL (Fig. 11b). Downdrafts were located just ahead of the updrafts. Consistent with the

weaker updrafts in a tropical oceanic environment, there was a sharp reflectivity gradient above the 0°C level. The forward tilt of radar reflectivity indicated the tendency of stratiform rain ahead of the system. From most previous observational (LeMone et al 1984, Jorgenson et al. 1997) and modeling (Trier et al. 1996) studies, it was found that a rearward tilting of the inflow was more common and usually resulting in a stratiform region trailing the convective part. In a recent climatological studies, Parker and Johnson (2000) found that the trailing or paralleling stratiform rain happens over 80% of convective lines observed in the United States, while the leading stratiform cases are only counted for 19%.

5. SUMMERY

During the first half of May 1998, the SCS regime was controlled by the Pacific subtropical high with low-level divergence and upper-level convergence. Although the frontal passage was periodically observed from the mainland China, as a result of unfavorable synoptic scale conditions, no systematic convection could develop in the SCS. The situation started to change on 15 May when two branches of southwesterly low-level tropical airflow arrived in the northern SCS. This was also an important mark for the onset of SEAM. Along with the development of the upper-level anticyclone over Indo-China to increase the upper level divergence in the region, the synoptic situation became favorable for the development of convection in the northern SCS. When a frontal system moved southeastward from mainland China over the sea, the associated rainband could maintain its intensity with localized enhancement. However, due to the onset of SEAM was limited in the northern SCS at its early stage, the convection failed to penetrate to the southern SCS region at that time. On 19 May, with the southward progression of SEAM onset, the next frontal system was able to extend further south and produce rain in a larger area. The onset of the SEAM at the upper level, a systematic northeasterly wind at the eastern flank of a well established anticyclone, was a longer process. During the onset period, an anticyclone over Indo-China moved northeastward. The development of the anticyclone turned westerly and northerly winds to northeasterly summer monsoon flow in most SCS region by 24 May, several days after the finish of monsoon onset at low-level. The following post-onset period to the end of SCSMEX included a short break period, a 10-day active period, and a long break period. This rainy period was a result of interaction between the southerly flow from tropics and the northerly flow from mid-latitude to generate a quasi-stationary low-level convergence zone. It is noted that during this active rainy period, the northern SCS area at the northeast corner of the upper-level anticyclone showed winds shift between northeasterly and westerly when the anticyclone vibrated between south and north. Following the retreat of the subtropical high in the western Pacific, the rain belt resulting from the low-level monsoon convergence zone jumped northward to southern China around 10 June. As a result, the Mei-Yu front formed in the Southern China and began a rainy period there. Meanwhile, the rainy period over the SCS region ended.

It was found that the interaction between the tropical monsoon flow and the frontal circulation played an important role to the organization and structure of the mesoscale convection on 15 May. The main convective line experienced a sharp orientation change from pre- to post-frontal regime. In the pre-frontal region, the earlier convection was embedded in the southwesterly flow regime. The primary convective line oriented perpendicular to the low-level wind shear, and the secondary convective lines were parallel to the low-level shear. This was in consistent with the conclusion made by LeMone et al. (1998) from their studies on western Pacific convection when the low-level wind shear is over 4 m s^{-1}. The maintenance and intensification of the convection relied on the low-level convergence of the different component of the southwesterly winds including the southwesterly monsoon flow and the original southwesterly frontal flow. In the post-frontal region, the later convection was formed by the southwesterly monsoon flow converging with the northerly frontal flow. Comparing to the pre-frontal convective line, the post-frontal convective line exhibited an east to west orientation, a sharp shift from northeast to southwest orientation. With the help of strong low-level convergence generated by the two branches of airflow at the opposite direction, the post-frontal convection was more intense and taller than the pre-frontal convection.

Comparing to the tropical MCS and squall lines documented in early literature, the cases studied here had significant departures from the archetypal concept model. Having intense convection with maximum radar reflectivity over 50 dBZ, the convection had little stratiform precipitation. It was believed to be related to the environmental conditions with very dry mid- to upper-level air and weak upper level winds. The hydrometers brought aloft by the updrafts would evaporate quickly in a super dry environment before forming a considerable area of stratiform rain. Meanwhile, the weak environmental winds at the upper level also limited the extension of the possible stratiform rain, as it would not blow the hydrometers away from the convective part. Different from the typical position of the stratiform rain that is usually behind its counterpart, the limited stratiform rain observed here was ahead of the convective core. This type of leading-stratiform mode seldom occurs over the land, and even more rare over the ocean. In a typical tropical convection, strong low-level convergence and updrafts are found in a narrow zone close to the leading

edge where the inflow interacts with the cold pool resulting from evaporation cooling. The new cells form ahead of the old ones. The low-level updrafts then go upward to the rear portion of the system and forming stratiform rain there. A large area of downdrafts is often observed behind the convective core. However, for the case of 15 and 24 May, the low-level convergence and updrafts were located in a wider area in the rear portion of the system. The new cells formatted behind the old ones. And, the updrafts turned forward like a return flow at the mid-to-upper levels and brought hydrometers ahead of the convective core. The downdrafts ahead of the updrafts were also evident. The new cell formation in the rear part implied that the low-level inflow had to pass a convective precipitating area. Consequently, the inflow could be chilled by the cool air caused by the evaporation cooling. This may reduce the strength of updrafts and have some negative effects on the development and maintenance of the convection. To maintain such an atypical kinematic structure, one of the following conditions should be met: a) there is a strong lifting along the edge of the cold surface outflow (case of 15 May), or b) the thermodynamic stratification is near neutral (case of 24 May).

ACKNOWLEDGEMENTS

The author would like to acknowledge those who participated in SCSMEX, especially Thomas Rickenbach (NASA/GSFC), Robert Cifelli (Colorado State University), Paul Kucera (University of Iowa), Tom Keenan (BMRC, Australia), and John Gerlach (NASA/WSFC) for their involvement in the radar observations and preliminary data processing. This research was supported by the NASA TRMM office and Mesoscale Atmospheric Research Branch.

REFERENCES

Biggerstaff, M. I. and R. A. Houze, Jr., 1991: Kinematic and precipitation structure of the 10-11 June 1985 squall line. *Mon. Wea. Rev.*, **119**, 3035-3065.

Chen, Y.-L., 1993: Some Synoptic-Scale Aspects of the Surface Fronts over Southern China during TAMEX. *Mon. Wea. Rev.*, **121,** 50–64.

Ding, Yihui, 1994: *Monsoons over China.* Kluwer Academic Publishers, 419 pp.

————, and Y. Liu, 2001: Onset and the evolution of the summer monsoon over the South China Sea during SCSMEX field experiment in 1998. *J. Meteorol. Soc. Japan*, **79**, 255-276.

Fu, C.-B., J. Fletcher, and R. Slutz, 1983: The structure of the Asian monsoon surface wind field over the ocean. *J. Climatol. Appl. Meteor.*, **22**, 1242-1252.

He, H., McGinnis, J. W., Song Z. S., Yanai, M., 1987: Onset of the Asian summer monsoon in 1979 and the effect of the Tibet Plateau. *Mon. Wea. Rev*., **115**, 1966-1995.

Houze, R. A., Jr., 1993: *Cloud Dynamics*. Academic Press, 573pp.

Johnson, R. H. and P. E. Ciesielski, 2002: Characteristics of the 1998 summer monsoon onset over the northern South China Sea. *J. Meteor. Soc. Japan*, **80**, 561-578.

————, and T. Keenan, 2001: Organization of oceanic convection during the onset of the 1998 East Asia summer monsoon. *30th International Conference on Radar Meteorology*. Preprints, Munich, Germany, Amer. Meteor. Soc., 679-681.

Jorgensen, D. P., M. A. LeMone, 1989: Vertical velocity characteristics of oceanic convection. *J. Atmos. Sci*., **46**, 621-640.

————, and ————, and S. B. Trier, 1997: Structure and evolution of the 22 February 1993 TOGA COARE squall line: aircraft observations of precipitation, circulation, and surface energy fluxes. *J. Atmos. Sci.*, **54**, 1961-1985.

Krishnamurti, T. N., 1985: Summer monsoon experiment—A review. *Mon. Wea. Rev*., **113**, 1590-1626.

Lau, K.-M., Y. Ding, J.-T. Wang, R. Johnson, T. Keenan, R. Cifelli, J. Gerlach, O. Thiele, T. Rickenbach, S. C. Tsay, and P.-H. Lin, 2000: Report of the field operations and early results of the South China Sea Monsoon Experiment (SCSMEX). *Bull. Amer. Meteor. Soc*., **81**, 1261-1270.

————, G. J. Yang, and S. H. Shen, 1988: Seasonal and intraseasonal climatology of summer monsoon rainfall over East Asia. *Mon. Wea. Rev*., **116**, 18-37.

Leise, J. A., 1981: A multidimensional scale-telescoped filter and data extension package. NOAA Tech. Memo. ERL WPL-82, 18 pp. [NTIS PB82-164104.]

LeMone, M. A., G. M. Barnes, E. J. Szoke, and E. J. Zipser, 1984: The tilt of the leading edge of mesoscale tropical convective lines. *Mon. Wea. Rev*., **112**, 510-519.

————, and E. J. Zipser, 1980: Cumulonimbus vertical velocity events in GATE. Part I: Diameter, intensity and mass flux. *Mon. Wea. Rev*., **108**, 2444-2457.

————, E. J. Zipser, and S. B. Trier, 1998: The role of environmental shear and thermodynamic conditions in determining the structure and evolution of mesoscale convective systems during TOGA COARE. *J. Atmos. Sci.*, **55**, 3493-3518.

Mohr, C. G., L. J. Miller, R. L. Vaughan, and H. W. Frank, 1986: The merger of mesoscale datasets into a common Cartesian format for efficient and systematic analyses. *J. Atmos. Oceanic. Technol*., **3**, 143-161.

Moncrieff, M. W., 1992: Organized convective systems: Archetypal dynamical models, mass and

momentum flux theory, and parameterization. *Quart. J. Roy. Meteor. Soc.*, **118**, 819-850.

Murakami, T., and Y. H. Ding, 1982: Wind and temperature changes over Eurasia during the early summer of 1979. *J. Meteorol. Soc. Japan*, **60**, 183-196.

Ninomiya, N. and T. Murakami, 1987: The early summer rainy season (Baiu) over Japan. *Monsoon Meteorology*, **93-121**. Chang, C.-P. and T.N. Krishnamurti, Eds., Oxford University Press, 353 pp.

Parker M. D. and R. H. Johnson, 2001: Simple numerical simulation of convective lines with leading stratiform precipitation. *Ninth Conference on Mesoscale Processes*. Preprints, Fort Lauderdale, FL, Amer. Meteor. Soc., 283-287.

Protat, A. and Y. Lemaitre 2001: Scale interaction involved in the initiation, structure, and evolution of the 15 December 1992 MCS observed during TOGA COARE. Part II: Mesoscale and convective-scale processes. *Mon. Wea. Rev.*, **129**, 1779-1808.

Tao, S. and Chen L., 1987: A review of recent research on the East Asian summer monsoon in China. *Monsoon Meteorology*, **60-92**. Chang, C.-P. and T.N. Krishnamurti, Eds., Oxford University Press, 353 pp.

Trier, S. B., W. C. Skamarock, M. A. LeMone, D. B. Parsons, and D. P. Jorgensen, 1996: Structure and evolution of the 22 February 1993 TOGA COARE squall line: Numerical simulations. *J. Atmos. Sci.*, **53**, 2861-2886.

Tu, Z.-W. and S.-S. Huang, 1944: The advance and retreat of the summer monsoon. *Meteor. Mag.*. **18**, 1-20.

Zipser, E. J., and M. A. LeMone, 1980: Cumulonimbus vertical velocity events in GATE. Part II: Synthesis and model core structure. *J. Atmos. Sci.*, **37**, 2458-2469.